

A Simple Algorithm for Orbit Classification

Eliza E. Fulton and Joshua E. Barnes[★]

Institute for Astronomy, 2680 Woodlawn Dr., Honolulu, HI 96822, USA

22 December 2018

ABSTRACT

We describe a simple algorithm for classifying orbits into orbit families. This algorithm works by finding patterns in the sign changes of the principal coordinates. Orbits in the logarithmic potential are studied as an application; we classify orbits into boxlet families, and examine the influence of the core radius on the set of stable orbit families.

Key words: celestial mechanics, stellar dynamics – galaxies: kinematics and dynamics – galaxies: structure

1 INTRODUCTION

The dynamical structure of an elliptical galaxy may be represented by a collection of orbits (e.g. Schwarzschild 1979). In this representation the time-average of each orbit yields an invariant density distribution, and a weighted sum of such distributions equals the overall mass density of the galaxy. Orbits are categorized into different families depending on their shapes; certain orbit families become stable or dominant in certain potentials. The orbits available in a given potential may be characterized in several interrelated ways. Classifying orbits into families says something about their geometry and thus about the contribution they can make to the mass distribution. This paper describes a simple algorithm for classifying orbits in elliptical potentials, and illustrates its application to the well-studied logarithmic potential (see Miralda-Escudé & Schwarzschild 1989, hereafter MES89).

The orbital content of triaxial potentials has long been of interest to dynamical astronomers. Integrable potentials have fairly simple structures, with one family of ‘box’ orbits and three of ‘tubes’ (de Zeeuw 1985). In nonintegrable potentials the situation is much more complex; chaotic orbits may appear (Goodman & Schwarzschild 1981; Valluri & Merritt 1998), and the monolithic tube and box families are partly replaced by a plethora of minor orbit families (Binney & Spergel 1982; MES89; Lees & Schwarzschild 1992). This rich structure is created by a pattern of resonances between fundamental orbital frequencies. In d dimensions there are d such frequencies ω_i , and an orbit family corresponds to a resonance condition of the form

$$\mathbf{n} \cdot \boldsymbol{\omega} = 0, \quad (1)$$

where \mathbf{n} is a vector of integers, and $|\mathbf{n}| > 0$; thus each orbit family may be characterized by the corresponding vector \mathbf{n} .

Several different approaches to orbit classification exist. Spectral methods (Binney & Spergel 1982, 1984; Papaphilippou & Laskar 1996, 1998; Carpintero & Aguilar 1998; Valluri & Merritt 1998) classify orbits by measuring their fundamental frequencies ω_i . These methods are powerful and general but also somewhat complex to implement. Alternately, orbits may be classified by heuristic methods based on known characteristics of specific orbit families. For example, tube orbits maintain a definite sense of circulation about a principal axis (e.g. Barnes 1992). Likewise, the ‘boxlet’ orbits found in nonintegrable potentials may be classified by measuring extrema along the principal coordinates (e.g. Schwarzschild 1993).

We have developed a classification algorithm that captures the geometry of both loop and boxlet orbits in a simple unified scheme. This algorithm is easily implemented and generalized to find higher-order resonances. In its present form the algorithm is best suited for two-dimensional potentials; while it provides a partial characterization of orbits in three-dimensional potentials, it cannot recognise the full range of orbit families present in such systems. Nonetheless, the generality and simplicity of our method may make it attractive when a full-blown spectral treatment is unnecessary or prohibitively expensive.

In this paper we describe the algorithm and present some sample results. Section 2 develops the theoretical basis for the algorithm and discuss some aspects of its implementation. Section 3 illustrates the use of this algorithm in exploring the orbits in the logarithmic potential. Conclusions and further applications of the algorithm are discussed in Section 4.

2 ALGORITHM

The key idea of our algorithm is to determine an orbit’s family from the pattern of sign changes of the principal coordinates (Barnes 1998, p. 352). This approach can be placed on

[★] E-mail: barnes@ifa.hawaii.edu

a firm foundation by examining sign-change patterns for the closed, stable orbits which parent an orbital family. A given family actually contains a one-parameter sequence of stable closed orbits, each with a different energy. In what follows we will use a single one of these closed orbits as representative of an entire family. This simplifies our exposition but has no other consequences, since all the closed orbits in a given family have the same topology and therefore the same sign-change pattern.

2.1 Closed orbits

In two dimensions, the resonance condition (1) establishes a unique relationship between the two fundamental frequencies of an orbit. We write (1) in the form

$$\ell\omega_x + m\omega_y = 0, \quad (2)$$

where ℓ and m are integers, and ω_x and ω_y are the orbital frequencies. We assume with no loss of generality (i) that the frequencies obey $0 < \omega_x \leq \omega_y$, (ii) that $m < 0 < \ell$, (iii) that m and ℓ are relatively prime, and (iv) that the orbit has a period of 2π . The resonance condition then implies that $\omega_x = -m$ and $\omega_y = \ell$.

Since ω_x/ω_y is a rational number, an orbit with two frequencies ω_x and ω_y will close on itself after a finite time. Such a closed orbit, if stable, can parent an orbital family. Although the motion is generally not harmonic, these closed orbits are topologically equivalent to Lissajous figures, which are parametric curves generated by

$$x(t) = \cos(\omega_x t), \quad y(t) = \cos(\omega_y t + \phi). \quad (3)$$

where $\phi \equiv k\pi/2\omega_y$ is a phase-shift. For any given ω_x and ω_y there are two values of the parameter k which yield possible parenting orbits: $k = 0$ generates the parents of boxlets, while $k = 1$ generates the parents of ‘antiboxlets’ (MES89).

Using the parametric equations (3), we can derive the pattern of sign changes of $x(t)$ and $y(t)$ for any distinct choice for (ℓ, m) and k . Since $\cos(\theta)$ has two sign changes for $\theta \in [0, 2\pi]$, this pattern is periodic with a period of π , or half the orbital period. We refer to the pattern generated over the interval $t \in [0, \pi]$ as the *semi-pattern*; in each semi-pattern $x(t)$ has $-m$ sign changes and $y(t)$ has ℓ sign changes. Before presenting a general treatment, we will discuss the semi-patterns of some key orbits, organized by their $\ell + m$ values. These examples also serve to introduce our notation for sign-change patterns.

2.1.1 The case $\ell + m = 0$

If $\ell = -m$ then since ℓ and m are relatively prime we have $(\ell, m) = (1, -1)$, so $\omega_x = \omega_y = 1$. In this case, the curve defined by (3) with $k = 0$ is trivial: a diagonal line passing through the origin. On the other hand, the curve produced with $k = 1$ is a circle, which is topologically equivalent to a loop orbit. For $t \in [0, \pi]$ the function $y(t)$ changes sign at $t = 0$, while $x(t)$ changes sign at $t = \pi/2$. Abstracting away the actual values of t but preserving the order of events, this orbit’s semi-pattern is represented by the string ‘YX’, where ‘Y’ marks a sign-change of $y(t)$ and ‘X’ a sign-change of $x(t)$. An orbit which produces a sign-change string of the form ‘YX’ repeated *ad infinitum* is a loop orbit.

2.1.2 The case $\ell + m = 1$

If $\ell = 1 - m$ and $k = 0$ then (3) yields ‘centrophobic’ orbits (MES89), which avoid the centre of the potential. The semi-pattern for such orbits is a string of the form ‘YX...Y’, in which $-m$ pairs of the symbols ‘YX’ are followed by a final ‘Y’. For example, the resonance $(\ell, m) = (2, -1)$ yields the semi-pattern ‘YXY’, and an orbit which produces a sign-change string consisting of infinite repetitions of ‘YXY’ is a centrophobic $(2, -1)$ resonance, also known as a ‘banana’ orbit (Binney 1982). Likewise, the resonance $(3, -2)$ yields ‘YXYXY’, which identifies a ‘fish’ orbit. Unlike the loop orbit described above, all semi-patterns of this kind must begin and end with the symbol ‘Y’. The sign-change string generated by an orbit of this kind will therefore contain places where the ‘Y’ appears twice with no intervening ‘X’. These doubled symbols have a simple physical interpretation: the angular momentum of the orbit reverses between the first and second ‘Y’.

In contrast, $k = 1$ yields ‘centrophilic’ orbits, which pass exactly through the centre of the potential. The simplest such orbit is the ‘antibanana’, produced by $(\ell, m) = (2, -1)$. For this orbit $y(t)$ has zeros at $t = 0$ and $\pi/2$, while $x(t)$ has a zero at $t = \pi/2$. To represent the simultaneous zeros of $x(t)$ and $y(t)$ at $t = \pi/2$, we surround the symbols with square brackets; thus the semi-pattern for this orbit is ‘Y[XY]’. Next is the ‘antifish’, produced by $(\ell, m) = (3, -2)$; the semi-pattern for this orbit is ‘YXY[XY]’. In all cases with $\ell + m = 1$, the semi-patterns for the centrophilic orbits resemble those of their centrophobic counterparts, except that the final symbols are ‘[XY]’, indicating that the orbit passes through the origin.

2.1.3 The case $\ell + m = 2$

If $\ell = 2 - m$ then $k = 0$ yields centrophilic orbits which pass through the origin at times just before $t = \pi/2$; thus the semi-patterns for such orbits contain a central ‘[XY]’ pair. The simplest orbit of this kind with $\omega_x/\omega_y \geq 1/2$ is $(\ell, m) = (5, -3)$, which produces the semi-pattern ‘YXY[XY]YXY’. The next resonance in this series, $(\ell, m) = (7, -5)$, yields ‘YXYXY[XY]YXYXY’. In general, each such pattern has three parts: the first is an alternating string of $(\ell - 1)/2$ copies of ‘Y’ and $(-m - 1)/2$ copies of ‘X’, the second is the central ‘[XY]’ pair, and the third is identical to the first.

For $k = 1$ we obtain centrophobic orbits. Each semi-pattern contains a total of ℓ copies of ‘Y’ symbols and $\ell - 2 = -m$ copies of ‘X’; thus within the semi-pattern two ‘Y’ symbols must appear next to each other. The simplest example is $(\ell, m) = (5, -3)$, which yields ‘YXYYXXY’. As already noted, ‘YY’ pairs indicate a reversal of the angular momentum; counting the two ‘Y’ symbols which begin and end the semi-period, we find that a centrophobic orbit with $\ell + m = 2$ reverses its sense of angular momentum four times before closing on itself.

2.1.4 General treatment

The coordinate functions $x(t)$ and $y(t)$ have zeros in the interval $t \in [0, \pi)$ at times

$$\begin{aligned}\tau_x &= \frac{\pi}{-m} \left(i_x + \frac{1}{2} \right), & i_x &= 0, 1, \dots, -m-1, \\ \tau_y &= \frac{\pi}{\ell} \left(i_y + \frac{1}{2} + \frac{k}{2m} \right), & i_y &= 0, 1, \dots, \ell-1.\end{aligned}\quad (4)$$

Using these expressions, it's straightforward to generate the semi-pattern for any given (ℓ, m) and k . Table 1 gives results for all resonances satisfying $\omega_x/\omega_y \geq 1/2$ which yield semi-patterns of 20 symbols or less. The resonances are grouped by $\ell + m$ value; within each group, they are sorted in order of increasing ω_x/ω_y ; finally we list the centrophobic version of each resonance before its centrophilic counterpart. The column labeled 'Key' gives a one-character symbol for each orbit family, which we will use in presenting results of orbit classification in Section 3.

In passing, we note a crucial fact: no semi-pattern consists of multiple copies of any other semi-pattern. This follows because ℓ and m are relatively prime.

The motion described by (3) is *reversible*; that is, the transformation $t \rightarrow -t$ leaves trajectories unchanged. Thus it may seem puzzling that some semi-patterns are not palindromes. The resolution of this puzzle lies in the fact that the transformation $t \rightarrow t + \Delta t$, where Δt is a constant, also leaves trajectories unchanged. Consequently, all cyclic permutations of a given semi-pattern should be identified with each other since they all represent the same trajectory. The reverse of a given semi-pattern can always be cyclicly permuted to obtain the original semi-pattern. We conclude that the asymmetric appearance of some semi-patterns is an artifact of our arbitrary choice for the origin of the time-line.

2.2 Family resemblances

The closed orbits in elliptical potentials are distorted versions of Lissajous figures, and each such figure yields a unique semi-pattern. We now argue that all the orbits in an orbital family yield similar sign-change patterns. Recall that in two dimensions, each orbit family is parented by a *stable* closed orbit. Stability is the key which enables an orbit to be a parent; informally, it implies that other orbits which start near the parenting orbit remain near it at later times. An orbital family is thus the set of all orbits which remain near a stable parenting orbit.

For a centrophobic family the resemblance is simple; all the orbits in a given family generate the *same* semi-pattern as does their parenting orbit. This seems intuitively clear for orbits which wander only a small distance from the path of their parent, but is it true for even the most far-flung family members? Yes, because no member of a centrophobic family passes exactly through the centre. Consider a continuous ensemble of family members which – up until now – have all generated the same sequence of x and y sign-changes, and are therefore at present all within the same (x, y) quadrant of the system. If some of these orbits next have sign-changes in x while others have sign-changes in y then the swath defined by their orbits must pass across the origin. But continuity then implies the ensemble includes orbits which pass exactly through the centre, which is impossible since the family is centrophobic.

On the other hand, a centrophilic family includes at least one member – the parenting orbit – which passes exactly through the centre every time. Other family members

Table 1. Semi-patterns of 20 symbols or less with $\omega_x/\omega_y \geq 1/2$.

ℓ	m	k	Key	Pattern
1	-1	1	L	YX
1	-1	0	1	[XY]
2	-1	0	b	YXY
2	-1	1	B	Y[XY]
3	-2	0	f	YXYXY
3	-2	1	F	YXY[XY]
4	-3	0	p	YXYXYXY
4	-3	1	P	YXYXY[XY]
5	-4	0	q	YXYXYXYXY
5	-4	1	Q	YXYXYXY[XY]
6	-5	0	r	YXYXYXYXYXY
6	-5	1	R	YXYXYXYXY[XY]
7	-6	0	s	YXYXYXYXYXYXY
7	-6	1	S	YXYXYXYXYXYXY[XY]
8	-7	0	t	YXYXYXYXYXYXYXY
8	-7	1	T	YXYXYXYXYXYXY[XY]
9	-8	0	u	YXYXYXYXYXYXYXY
9	-8	1	U	YXYXYXYXYXYXYXY[XY]
10	-9	0	v	YXYXYXYXYXYXYXYXY
10	-9	1	V	YXYXYXYXYXYXYXYXY[XY]
5	-3	1	@	YXYXYXY
5	-3	0	2	YXY[XY]YXY
7	-5	1	#	YXYXYXYXYXY
7	-5	0	3	YXYXY[XY]YXYXY
9	-7	1	\$	YXYXYXYXYXYXYXY
9	-7	0	4	YXYXYXY[XY]YXYXYXY
11	-9	1	%	YXYXYXYXYXYXYXYXY
11	-9	0	5	YXYXYXYXY[XY]YXYXYXY
7	-4	0	w	YXYXYXYXYXY
7	-4	1	W	YXYXY[XY]YXY
8	-5	0	x	YXYXYXYXYXYXY
8	-5	1	X	YXY[XY]YXYXYXY
10	-7	0	y	YXYXYXYXYXYXYXY
10	-7	1	Y	YXYXYXYXYXY[XY]YXYXY
11	-8	0	z	YXYXYXYXYXYXYXYXY
11	-8	1	Z	YXYXY[XY]YXYXYXYXYXY
9	-5	1	&	YXYXYXYXYXYXY
9	-5	0	7	YXYXY[XY]YXYXY
11	-7	1	*	YXYXYXYXYXYXYXY
11	-7	0	8	YXYXYXY[XY]YXYXYXY
11	-6	0	g	YXYXYXYXYXYXYXY
11	-6	1	G	YXYXYXYXY[XY]YXYXY
12	-7	0	h	YXYXYXYXYXYXYXY
12	-7	1	H	YXYXYXYXYXYXYXY[XY]YXY
13	-7	1	?	YXYXYXYXYXYXYXYXY
13	-7	0	0	YXYXYXYXY[XY]YXYXYXY

come arbitrarily close to the centre, but generally pass to one side or the other; the swath defined by an ensemble of such orbits has finite width as it crosses the origin. Thus some of members of the ensemble have sign-changes in the order 'XY' and some in the order 'YX', while only a infinitesimal subset pass exactly through the centre and produce '[XY]'. The sign-change sequence generated by a typical centrophilic family member is an infinite repetition of its parenting orbit's semi-pattern with one embellishment – where the parent's semi-pattern contains '[XY]' the member's realization may contain either 'XY' or 'YX' (but not 'XX' or 'YY'). Thus, each '[XY]' indicates a place where the order of the symbols is interpreted as *ambiguous*.

This interpretation complicates matters, since the semi-pattern of a centrophobic resonance will match the semi-pattern of its centrophilic counterpart. Nonetheless, an orbit can be assigned to its appropriate family with little ambiguity – given a sufficiently long sequence of sign-change data generated by following the orbit’s trajectory. Match the orbital data against each semi-pattern in turn, taking care to test centrophobic resonances before testing centrophilic ones; the first successful match gives the orbit’s family. With a finite sequence of sign-change data, it’s possible that a centrophilic resonance will be miss-classified as centrophobic, but the probability of such an error is small if enough trajectory data is available.

2.3 Implementation

A fairly straightforward computer program serves to implement the algorithm outlined above. This program computes the trajectory $(x(t), y(t))$ of an orbit, recording the sign-changes of x and y ; once a total of N_{change} sign-changes have been recorded, these are matched against a finite set of semi-patterns. A successful match identifies the orbit’s family. If none of the semi-patterns match the orbit’s sign-change data then the latter are searched for *any* strictly periodic pattern of length $\leq L_{\text{max}}$; this catches all centrophobic families with $\ell - m \leq L_{\text{max}}$. If no such pattern is found then the orbit may be a higher-order resonance, a true (regular) box with incommensurate ω_x and ω_y , or a stochastic orbit; our algorithm can’t distinguish between these possibilities.

The trajectory-following section of the program is built around a 4th-order RK integrator with a time-step always proportional to the local dynamical time. While a higher-order integrator and local error control would improve the accuracy of the computed trajectories, convergence tests indicate that most orbits can be robustly classified even when integrated with energy errors as large as 0.1 per cent; to be on the safe side, we limit the peak-to-peak energy variation to 0.02 per cent. After each time-step, the new values of x and y are compared with their previous values; if one has changed sign then this event is recorded, while if both have changed sign then both events are recorded, with linear interpolation used to determine which occurred first. The algorithm does not try to detect passages exactly through the origin; such passages are vanishingly rare.

The semi-patterns used to try and match the sign-change data are generated from the (ℓ, m) and k values stored in a table like Table 1. When matching the orbital data to a semi-pattern we demand symbol-by-symbol equality throughout unless the semi-pattern contains ‘[XY]’; at that point the orbital data may contain either ‘XY’ or ‘YX’. One final subtlety about the matching routine is worth mentioning: since the phase of the orbital data is indeterminate, it is matched against all cyclic permutations of each semi-pattern. Even with this added complication, the amount of computer time spent matching orbital data to patterns is insignificant; only integer arithmetic is required, and most possible matches are quickly rejected.

Finally, the routine which checks the orbital data for arbitrary periodic patterns is quite simple. To test for a semi-pattern of length L we take the first L symbols as the model and match them against the rest of the data. In this matching process it’s not necessary to consider cyclic per-

mutations of the semi-pattern since it automatically has the same phase as the orbit. If the match succeeds, the ℓ and m values of the parenting resonance are determined by counting the number of ‘Y’ and ‘X’ symbols, respectively, in the semi-pattern. If the match fails then the routine next checks for semi-patterns of length $L + 1, \dots, L_{\text{max}}$.

The availability of this final ‘safety-net’ for arbitrary periodic patterns poses an interesting question: do orbit integrations ever yield periodic sign-change sequences which can’t be generated by the scheme in Section 2.1? No evidence for such orbits has been found. For example, Table 1 contains all semi-patterns of length $L \leq 20$ which can be generated by the scheme. Among the many thousands of 2-D orbits studied in the next section we have found *none* with periodic semi-patterns of length $L \leq 20$ which are not in Table 1. This success illustrates the power of MES89’s *ansatz* linking periodic orbits to Lissajous figures.

3 APPLICATION

To demonstrate the use of our algorithm we made a survey of orbits in the logarithmic potential,

$$\Phi = \frac{1}{2} \ln \left(R_c^2 + x^2 + \frac{y^2}{b^2} \right), \quad (5)$$

with ellipticity $b \leq 1$ and core radius R_c (Richstone 1980; Binney & Tremaine 1987; MES89). The goal of this survey was to show how the core radius influences the set of orbit families. We focused on orbits of total energy

$$E \equiv \Phi(\mathbf{r}) + \frac{1}{2} |\dot{\mathbf{r}}|^2 = 0. \quad (6)$$

This restriction to $E = 0$ is largely a matter of convenience. In a singular logarithmic potential ($R_c = 0$) an orbit with $E \neq 0$ can always be rescaled to one with $E = 0$. If $R_c \neq 0$ then rescaling is still possible if the core radius changes along with the energy so that $E - \ln R_c$ stays constant. Thus fixing E and changing R_c , as we do in Section 3.2, is equivalent to fixing R_c and changing E , and no new orbital families would come to light if we were to vary *both* parameters instead of just one.

In designing an orbit survey, perhaps the most critical choice is the ‘start space’ which samples the manifold of possible orbits. Below we examine several possible choices. First, we present results for a two-dimensional start space which is guaranteed to include all orbits but awkward to use when surveying a large number of potentials. Second, we present results for several one-dimensional start spaces which between them allow access to all known orbits.

3.1 2-D start space

The phase space for a two-dimensional potential has four dimensions: two positions, (x, y) , and two velocities, (\dot{x}, \dot{y}) . Since all orbits eventually cross the y axis, we stipulate that the initial x coordinate is $x_0 = 0$. The equation for E above then fixes any one of the remaining coordinates in terms of the other two. We constructed a grid in y_0 and \dot{y}_0 , and found \dot{x}_0 using (6). The resulting two-dimensional start space is parameterized by the same coordinates often used when con-

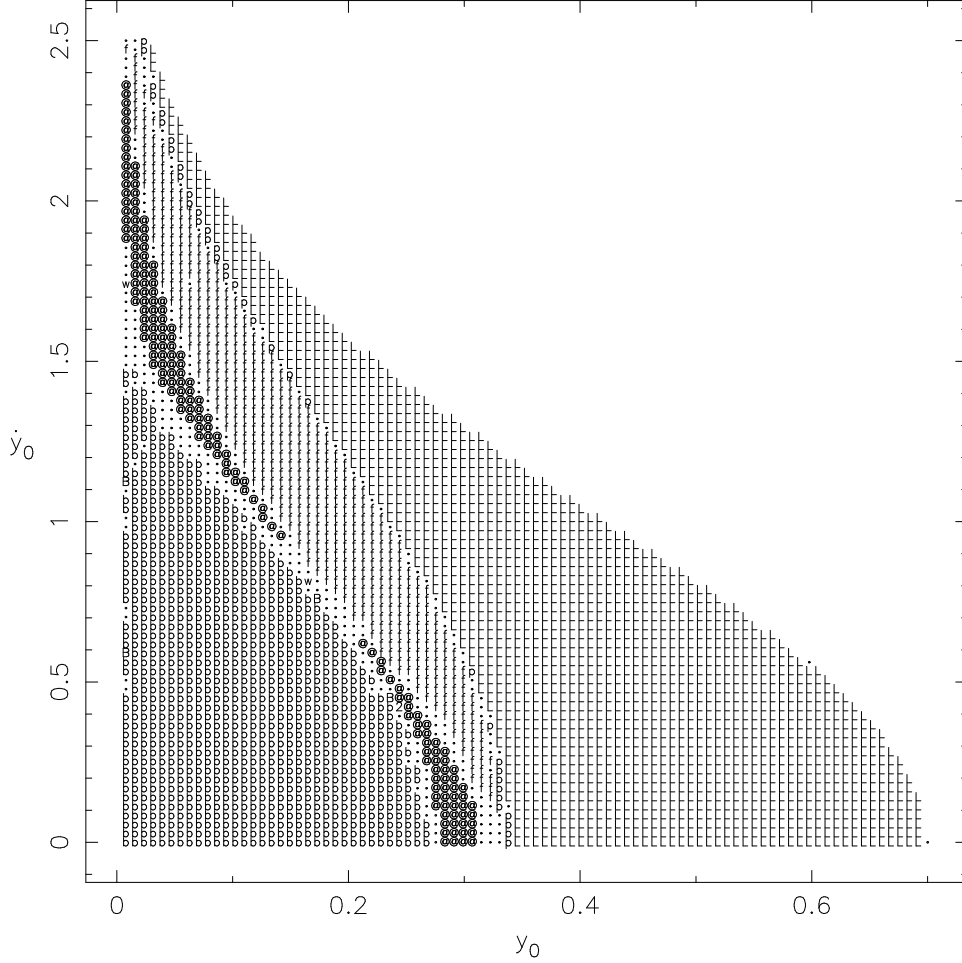


Figure 1. Orbit families accessible from the 2-D start space. The potential has core radius $R_c = 0$ and ellipticity $b = 0.7$. The symbol plotted at each grid point indicates the classification according to the ‘Key’ in Table 1.

structing a ‘surface of section’ (Hénon & Heiles 1964; Contopoulos 1983; Binney & Tremaine 1987, p. 117).

Fig. 1 shows the result of classifying orbits in the logarithmic potential with core radius $R_c = 0$ and ellipticity $b = 0.7$ using this two-dimensional start space. We emphasise that this diagram is *not* a surface of section; rather than plotting an orbit’s position on the (y, \dot{y}) plane each time it intersects $x = 0$, we plotted the results of classifying separate orbits launched from each point on the grid. We use the symbols listed in the ‘Key’ column of Table 1 to indicate the classifications, with a small dot marking orbits which don’t belong to any family with $\ell - m \leq 20$. Our result may be directly compared to those of other orbit-classification schemes (Carpintero & Aguilar 1998, Fig. 16) and to the traditional surface of section for this potential (MES89, Fig. 1); the agreement is very good. Basically, the phase space for this potential is almost entirely occupied by a few centrophobic orbit families. Starting at the lower left we find a large number of $(\ell, m) = (2, -1)$ banana orbits. Moving diagonally across the plot, we next encounter a strip, broken in the middle, of $(5, -3)$ resonances. Next comes a region of $(3, -2)$ fish orbits, followed by a narrow

strip of $(4, -3)$ pretzel orbits. Finally, the right-hand side of the plot is entirely occupied by $(1, -1)$ loop orbits.

The classifications shown in Fig. 1 were made using $N_{\text{change}} = 1000$ sign-changes per orbit. This gives a high level of confidence; for example, every fish orbit in this diagram has executed 200 semi-patterns without a single sign-change out of place. Since the orbit families in this particular potential all have fairly short semi-patterns, we could have obtained results almost as good with less than 100 sign-changes per orbit. A potential which supports a wider range of resonances provides a more stringent test of the classifier. We therefore chose a potential with $R_c = 0.02$ and $b = 0.8$; compared to the potential used for Fig. 1, the finite core radius helps stabilize centrophilic orbits, while the more modest flattening favors high-order resonances. The same orbits were independently classified for $N_{\text{change}} = 125, 250, 500$, and 1000, and the results compared to determine which orbit classifications are sensitive to this parameter. Even with $N_{\text{change}} = 125$, the $(\ell, m) = (2, -1), (5, -3), (3, -2)$, and $(4, -3)$ resonances were accurately classified, but incorrect classifications sometimes resulted for higher resonances such as $(9, -5), (7, -4), (8, -5)$, and $(7, -5)$. We observed two kinds of classification errors: false positives from non-

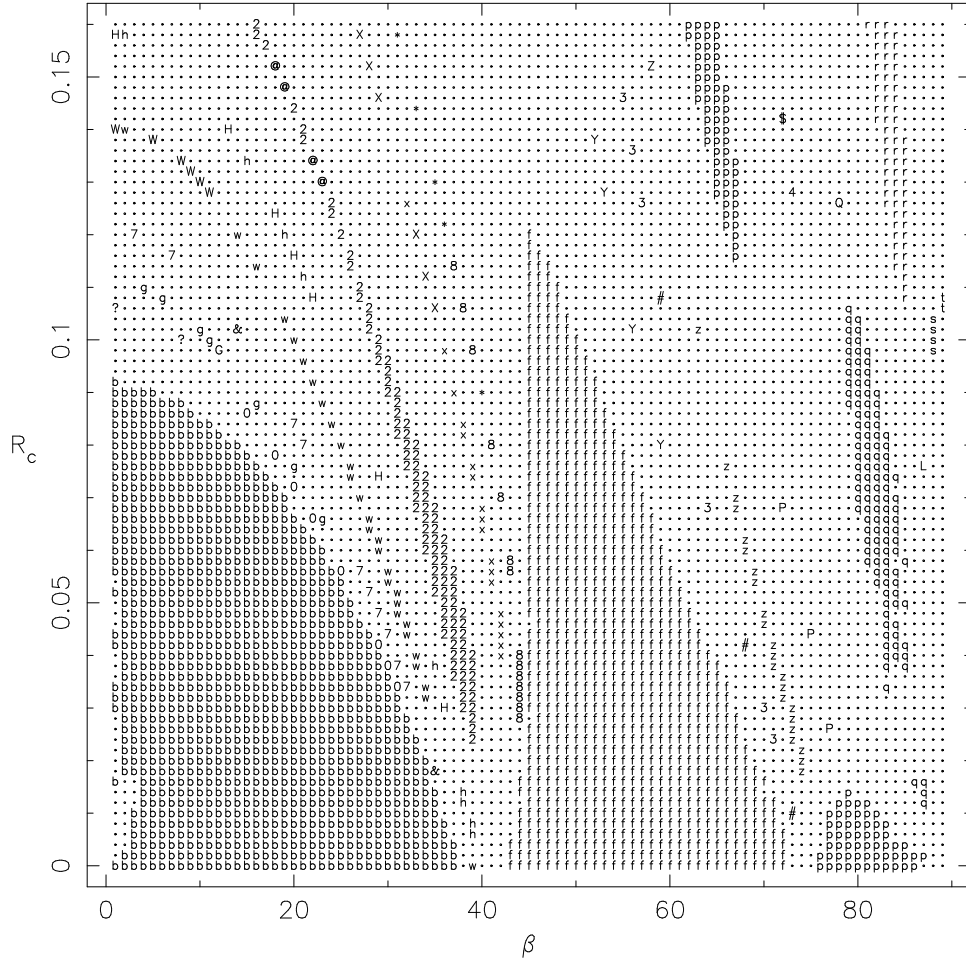


Figure 2. Orbit families accessible from the stationary start space. The potential has ellipticity $b = 0.8$. The vertical axis shows R_c , the core radius, while the horizontal axis shows β , the angular coordinate of the initial position.

resonant orbits which happen to lie *near* stable resonances, and mistaken identities due to confusion between centrophobic and centrophilic versions of the same resonance. The output of the classifier converges nicely as N_{change} is increased; taking the results for $N_{\text{change}} = 1000$ as fiducial, we find total error rates of 4.3, 1.9, and 0.8 per cent, for $N_{\text{change}} = 125$, 250, and 500, respectively.

3.2 1-D start spaces

In most previous studies of boxlets the initial conditions were generated by choosing initial positions \mathbf{r}_0 on the equipotential surface $\Phi(\mathbf{r}_0) = E$ and setting the initial velocities $\dot{\mathbf{r}}_0$ to zero. This ‘stationary’ start space yields a wide variety of boxlets, but it excludes orbits like the antifish which don’t have a stationary point – that is, a point at which $|\dot{\mathbf{r}}| = 0$. Alternatively, if the potential is finite at the origin one may consider setting the initial positions \mathbf{r}_0 to zero and choosing initial velocities satisfying $|\dot{\mathbf{r}}_0| = (2E - 2\Phi(0))^{1/2}$ (Papaphilippou & Laskar 1996). This ‘central’ start space includes the antifish, but it excludes centrophobic orbits. When using the stationary start space we parameterize the initial position in terms of the angle β between \mathbf{r}_0 and the x

axis; likewise when using the central start space we parameterize the initial velocity in terms of the angle β' between $\dot{\mathbf{r}}_0$ and the x axis.

Fig. 2 presents a survey of the stationary start space for logarithmic potentials with ellipticity $b = 0.8$ and core radii R_c in the range 0.16 to 0.0. As in Fig. 1, the result of each orbit classification is shown using the symbols listed in Table 1. For the larger values of R_c boxlets are few and far between, with only the $(\ell, m) = (4, -3)$ and $(6, -5)$ resonances occupying more than a handful of orbits. As R_c decreases, low order resonances such as $(2, -1)$ and $(3, -2)$ appear and grow in importance, eventually dominating the start space as $R_c \rightarrow 0$. The general trend with core radius seen here is entirely consistent with the results presented by MES89.

Although the overall outline of Fig. 2 is unsurprising, some of the higher-order resonances present in this diagram may be less familiar. For example, there is a narrow band of centrophilic $(\ell, m) = (5, -3)$ orbits extending from the top of the diagram and ending near $R_c \simeq 0.02$ and $\beta \simeq 39^\circ$. This family is distinct from the centrophobic $(5, -3)$ resonance seen in Fig. 1 and in previous studies (MES89; Lees & Schwarzschild 1992). In addition, this centrophilic family

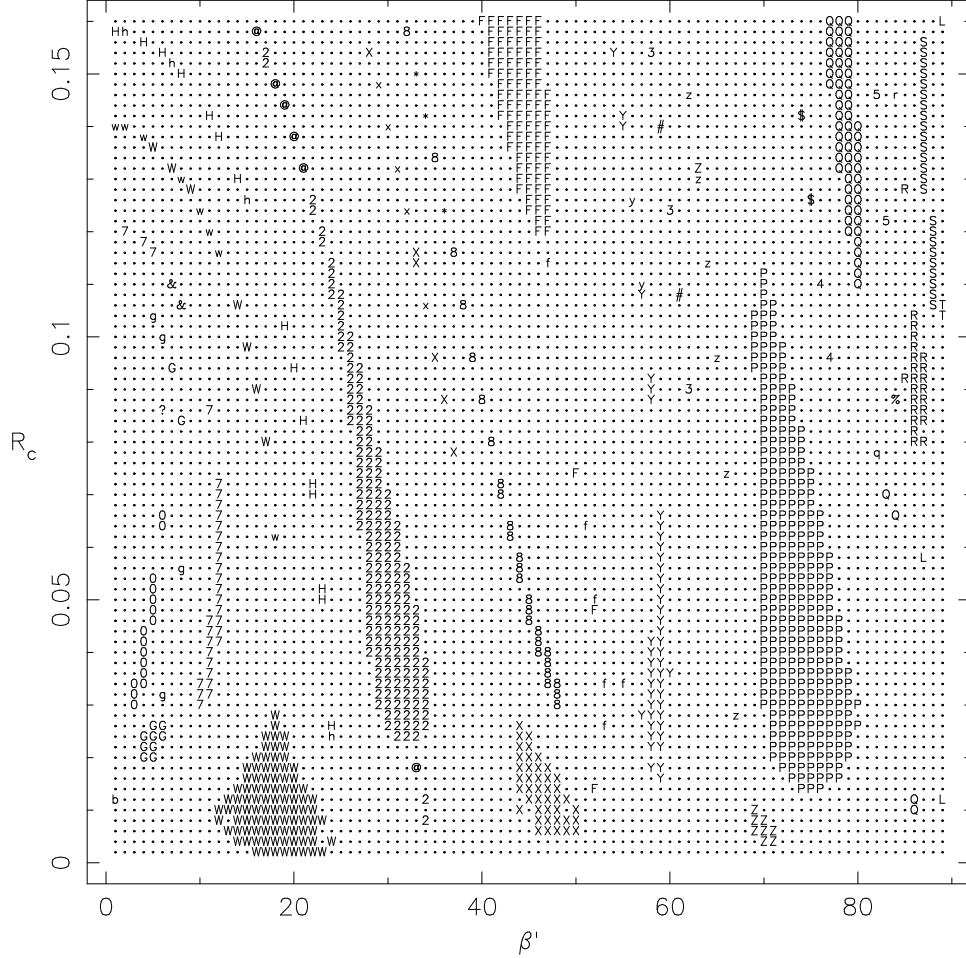


Figure 3. Orbit families accessible from the central start space. The potential has ellipticity $b = 0.8$. The vertical axis shows R_c , the core radius, while the horizontal axis shows β' , the angular coordinate of the initial velocity.

is flanked on either side by two centrophobic higher-order resonances: the $(7, -4)$ and $(8, -5)$ families. Only the former has been noted in the literature (Lees & Schwarzschild 1992), but the overall pattern seen here might have been anticipated since rational numbers, each corresponding to a possible resonance, are dense among the reals. The pattern of resonant orbits in Fig. 2 may be summarized as follows: at some starting angle β between any two resonances, (ℓ_1, m_1) and (ℓ_2, m_2) , one may look for a resonance of the form $(\ell_1 + \ell_2, m_1 + m_2)$. Of course, not all resonances are stable, and unstable resonances don't parent orbit families. Nonetheless, we expect that much of the space in Fig. 2 occupied by unclassified orbits (dots) is actually threaded by a fine array of still higher-order families.

But Fig. 2 can't capture all the stable resonances; it only shows orbits which have a stationary point. In Fig. 3, constructed using a central start space, we partly remedy this deficiency; this plot includes *all* centrophilic orbits, both those that have stationary points and those that do not. We find a number of new orbit families. For larger values of R_c there is a region of $(\ell, m) = (3, -2)$ orbits (antifish) centred on $\beta' \simeq 45^\circ$, and a narrow strip of $(5, -4)$ orbits near $\beta' \simeq 78^\circ$. At intermediate values of R_c there is a fairly

wide region of $(4, -3)$ resonances (antipretzels) near $\beta' \simeq 75^\circ$. Finally, the bottom part of the plot contains regions of $(7, -4)$ resonances near $\beta' \simeq 18^\circ$ and $(8, -5)$ resonances near $\beta' \simeq 47^\circ$. These families, and several others, are not represented in Fig. 2.

Together, Figs. 2 and 3 exhibit an interesting regularity; as R_c changes, a given boxlet vanishes from one plot at almost the same point where the corresponding antiboxlet appears in the other, and *vice versa*. For example, the centrophilic $(\ell, m) = (3, -2)$ family is confined to $R_c \gtrsim 0.12$, while the centrophobic version of the same family is confined to $R_c \lesssim 0.12$. A similar statement applies to the pair of $(4, -3)$ resonances and to other pairs of resonances as well. This behavior can be understood from MES89's discussion of bifurcations in the logarithmic potential; they remark that as a function of R_c , 'a boxlet and its antiboxlet change stability in such a manner that generally one is stable and the other is unstable'.

Does this rule extend to all resonances? The centrophilic $(\ell, m) = (5, -3)$ family is seen in both Figs. 2 and 3 for $R_c \gtrsim 0.02$, but neither plot shows the complementary family. This is easily explained; the missing family is centrophobic and has no stationary point, so it's automatically excluded

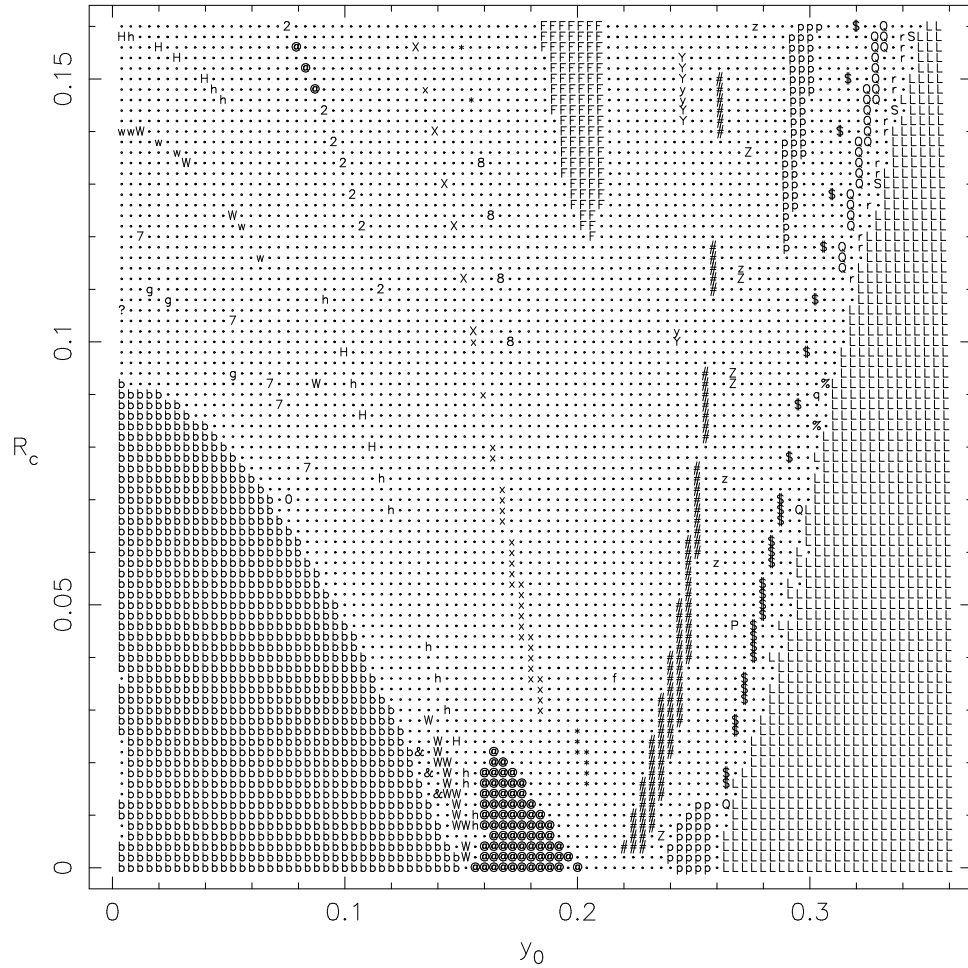


Figure 4. Orbit families accessible from the perpendicular start space. The potential has ellipticity $b = 0.8$. The vertical axis shows R_c , the core radius, while the horizontal axis shows y_0 , the initial position along the minor axis.

from both plots. We therefore constructed a ‘perpendicular’ start space by setting $x_0 = \dot{y}_0 = 0$ and using (6) to fix \dot{x}_0 in terms of y_0 . This start space allows access to centrophobic orbits which don’t have a stationary point – provided that each orbit at some point crosses the y axis at an angle of 90° . Fig. 4 shows the results of classifying orbits from this start space for y_0 in the range 0.004 to 0.36. (We excluded the axial orbit obtained with $y_0 = 0$, and trimmed off the loop orbits which dominate this start space from $y_0 \simeq 0.3$ out to the maximum value, $y_{\max} = b(1 - R_c^2)^{1/2} \simeq 0.8$.) This new plot shows the missing centrophobic $(5, -3)$ family appearing as expected for $R_c \lesssim 0.02$; it’s centred on $y_0 \simeq 0.18$. Several other families in Fig. 4 also reinforce this pattern; for example, the small clutch of centrophobic $(11, -7)$ orbits centred on $y_0 \simeq 0.2$, $R_c \simeq 0.02$ neatly complements the narrow bands of centrophilic $(11, -7)$ orbits which extend down to $R_c \simeq 0.03$ in Figs. 2 and 3.

Fig. 4 also shows several families previously undetected. The centrophobic $(\ell, m) = (7, -5)$ resonance occupies a strip extending from $y_0 \simeq 0.22$ at the bottom of the plot to $y_0 \simeq 0.26$ at the top. This strip has appreciable width for smaller core radii but narrows to less than the space between adjacent grid points in y_0 for $R_c \gtrsim 0.08$, thereby creating

apparent gaps where the strip misses the grid. A similar effect is seen in the centrophobic (9, -7) family. Both of these families seem stable for almost all – if not quite all – values of R_c tested, so it's probably not worth looking for their centrophilic counterparts.

4 DISCUSSION

Our algorithm works by reducing orbital trajectories to sequences of symbols, and matching these sequences against a set of known patterns. The idea of describing trajectories symbolically is not new; it has been applied to geodesics on negatively-curved surfaces, to forced van der Pol oscillators, and to the restricted three-body problem (Moser 1973 and references therein). Symbolic representation of orbits may have other applications in galactic dynamics. Below we briefly discuss a few related issues and some possible future developments.

4.1 Start spaces

The reader may feel somewhat reassured to learn that the three 1-D start spaces considered above are probably both

necessary and *sufficient* to find all boxlet families. We can show this by using the properties of the parametric curves (3). First, the orbits which have stationary points are those for which $k = 0$. Second, centrophilic orbits are those for which the quantity $\ell + m + k$ is an even number. Third, orbits which cross the y axis at an angle of 90° are those for which $\ell + 2m + k$ is even. Now if an orbit has no stationary point and is centrophobic then it has $k = 1$ and $\ell + m + k$ is odd, and because ℓ and m are relatively prime it follows that m is odd and $\ell + 2m + k$ is even – so the orbit crosses the y axis at 90° . Thus *any* orbit must fall into at least one of these three categories. Orbits with $k = 0$ can be accessed from the stationary start space, orbits with even $\ell + m + k$ are reachable using the central start space, and orbits with even $\ell + 2m + k$ result from the perpendicular start space. With a few exceptions due to misclassification of high-order resonances, these rules accurately predict which orbit families appear in each of Figs. 2, 3, and 4.

The stationary and perpendicular start spaces suffice for the singular logarithmic potential ($R_c = 0$) since all centrophilic orbits are unstable in this potential (e.g. Kuijken 1993).

These results have some bearing on orbit surveys in three-dimensional potentials. At a given energy, the manifold of possible orbits can be covered by a 4-D start space constructed by analogy with the 2-D start space described in Section 3.1 (Levison & Richstone 1987). Since this start space is awkward to sample and to display, many workers favor 2-D start spaces analogous to the stationary and perpendicular start spaces described above (Schwarzschild 1993). But these 2-D start spaces don't allow access to centrophilic orbits which lack a stationary point, and these orbits may be stable in nonsingular potentials. Thus a full survey of orbits in a three-dimensional nonsingular potential requires *at least* three different 2-D start spaces: the stationary and perpendicular start spaces must be supplemented by a central start space (Merritt 1999). It still remains to be shown that these 2-D spaces really are sufficient to access all orbits.

4.2 Noninteger k ?

We've assumed, following MES89, that the *only* allowed values of the phase parameter are $k = 0$ and $k = 1$. This assumption is critically important for the discussion in the previous subsection. However, D. Merritt (private communication) has pointed out that k may have values between 0 and 1; for example, in a 2-D harmonic oscillator the x and y motions are independent and neutrally stable orbits with *any* real value of k exist. For nonintegrable potentials the situation is unclear; k is probably limited to a discrete set of values, but it's possible that values between 0 and 1 are permitted. Our algorithm can't distinguish a resonant orbits with noninteger k from a centrophobic orbit with the same (ℓ, m) , since both yield the same sign-change pattern. Such orbits would be excluded from the 1-D start spaces used in Section 3.2, though in principle they are accessible from a 2-D start space. Visual inspection may be the easiest way to discover orbits with noninteger k ; such orbits, while following the same sign-change patterns as 'normal' centrophobes, would have different symmetry properties. No such orbits have been seen in a cursory inspection of candidates, but more work is needed.

4.3 Orbit families

The results presented in Section 3 emphasize the remarkable variety and structure of orbit families in the logarithmic potential. Of the 46 families listed in Table 1, some 29 can be found in Figs. 2, 3, and 4. Almost half of these families are centrophilic. While centrophilic orbits have been described before (MES89; Lees & Schwarzschild 1992; Barnes 1998, Fig. 42), most earlier studies treated these families as isolated curiosities. MES89's bifurcation diagrams showed that boxlets and antiboxlets exchange parental roles as R_c changes; we have made the consequences of this role-reversal visible by routinely finding the centrophilic counterparts of unstable centrophobic orbits. Centrophilic orbits may be destabilized by central mass concentrations in real galaxies, but their recognition still helps in understanding the mechanisms which determine the orbital content of a potential.

We note that some families did not appear in any of our classification diagrams. Most of these missing families are fairly high-order resonances which may be difficult to find because they occupy very small regions of the start spaces. Two low-order centrophilic families, however, are conspicuously absent. One is the orbit generated by the $(\ell, m) = (1, -1)$ resonance with $k = 0$, and the other is the antibanana, generated by the $(2, -1)$ resonance with $k = 1$. The former resonance is stable in some anharmonic potentials (de Zeeuw & Merritt 1983), while the latter may occur in highly flattened logarithmic potentials (Papaphilippou & Laskar 1996, Fig. 10). We would not expect these centrophilic orbits to appear in our plots since their centrophobic counterparts, the loop and banana orbits, do appear and are stable for a wide range of parameters.

4.4 3-D orbits

It's somewhat disappointing to admit that the technique described here doesn't trivially generalize to three-dimensional potentials. The reason for this failure is fairly straightforward. In two dimensions the resonance condition (1) fixes a unique relation between the fundamental frequencies, but in three dimensions it does not; as a result, the parenting orbits of many three-dimensional orbit families are thin membranes rather than closed curves (Merritt & Valluri 1999). Such parenting orbits don't generate unique periodic sign-change sequences, so our present algorithm can't recognise them. In contrast, spectral methods work quite well in three dimensions (Carpintero & Aguilar 1998; Papaphilippou & Laskar 1998; Valluri & Merritt 1998).

Nonetheless, we can partly classify orbits in three-dimensional potentials by projecting their trajectories onto the principal planes and using our two-dimensional algorithm to analyse the resulting sign-change sequences. This approach recognises resonances in which one component of the integer vector \mathbf{n} in (1) is zero; such resonances, though not the rule, are fairly common in many potentials (Papaphilippou & Laskar 1998; Merritt & Valluri 1999). Some orbits obey two independent resonance conditions; such 'doubly-degenerate' orbits are parented by closed three-dimensional curves. But even doubly-degenerate orbits don't always yield strictly periodic sign-change sequences. For example, the centrophobic 'banana-pretzel' orbit, combining a $(2, -1)$ resonance in the $x-z$ plane with a $(4, -3)$ resonance

in the x - y plane, yields a ‘ZYXZ[YZ]X[ZY]ZXYZ’ semi-pattern containing not one but *two* ambiguously-ordered pairs of symbols. This example suggests that more general pattern-matching methods may be able classify the crossing-sequences generated by arbitrary three-dimensional resonances.

4.5 Future developments

There are several ways in which this algorithm could be improved or extended. As just mentioned, one line of attack is to generalize the pattern-scanning process. It seems fairly easy to extend the routine which searches for arbitrary periodic patterns (Section 3.2) to recognise centrophilic as well as centrophobic semi-patterns; this would provide a better safety-net for high-order resonances. It’s also straightforward, in principle, to couple the trajectory-following and pattern-matching routines together so that the latter can call the former as needed for more data to resolve ambiguous cases. This would be more efficient and reliable than first integrating the orbit for a fixed number of sign-changes and then analysing the results.

Another line of attack is to adapt the algorithm to analyse N-body simulations. A simplified version has already been used to classify orbits in merger remnants (Barnes 1998; Bendo & Barnes 2000); however, this version just followed individual trajectories in a frozen approximation of the N-body potential. A more interesting project would be to classify orbits directly from the computed trajectories in a simulation. This could be accomplished by using an N-body code to generate separate sign-changes sequences for all N bodies; these sequences could be quickly scanned by pattern-matching algorithms like the one described here. Such techniques could attach a concise historical record to each body in an N-body simulation, nicely complementing the instantaneous snapshots of positions and velocities which currently form the basis for most N-body analysis.

We thank the referee, Dr. P. Palmer, for an open and constructive report, and L. Aguilar, T. de Zeeuw, D. Merritt, and E. Roberts for valuable and encouraging comments on a preliminary draft of this paper. This work was supported in part by NASA grant NAG 5-8393 and STScI grant GO-06430.03-95A.

REFERENCES

Barnes, J.E. 1992, *ApJ*, 393, 484
 Barnes, J.E. 1998, *Galaxies: Interactions and Induced Star Formation*, eds. D. Friedli, L. Martinet, D. Pfenniger (Springer-Verlag, Berlin), p. 275
 Bendo, G.J., Barnes, J.E. 2000, *MNRAS*, in press
 Binney, J. 1982, *MNRAS*, 201, 1
 Binney, J., Spergel, D. 1982, *ApJ*, 252, 308
 Binney, J., Spergel, D. 1984, *MNRAS*, 206, 159
 Binney, J., Tremaine, S. 1987, *Galactic Dynamics* (Princeton: Princeton University Press)
 Carpintero, D. D., Aguilar, L. A. 1998, *MNRAS*, 298, 1
 Contopoulos, G. *A&A*, 117, 89
 de Zeeuw, P.T. 1985, *MNRAS*, 216, 273
 de Zeeuw, T., Merritt, D. 1983, *ApJ*, 267, 571
 Gerhard, O. E., Binney, J. J. 1985, *MNRAS*, 216, 467
 Goodman, J., Schwarzschild, M. 1981, *ApJ*, 245, 1087
 Hénon, M., Heiles, C. 1964, *AJ*, 69, 73
 Kuijken, K. 1993, *ApJ*, 409, 68
 Lees, J.F., Schwarzschild, M. 1992, *ApJ*, 384, 491
 Levison, H.F., Richstone, D.O. 1987, *ApJ*, 314, 476
 Merritt, D. 1999, *PASP*, 111, 129
 Merritt, D., Valluri, M. 1999, *AJ*, 118, 1177
 Miralda-Escudé, J., Schwarzschild, M. 1989, *ApJ*, 339, 752
 Moser, J. 1973, *Stable and Random Motions in Dynamical Systems*, (Princeton: Princeton University Press)
 Papaphilippou, Y., Laskar, J. 1996, *A&A*, 307, 427
 Papaphilippou, Y., Laskar, J. 1998, *A&A*, 329, 451
 Richstone, D.O. 1980, *ApJ*, 238, 103
 Schwarzschild, M. 1979, *ApJ*, 232, 236
 Schwarzschild, M. 1993, *ApJ*, 409, 563
 Valluri, M., Merritt, D. 1998, *ApJ*, 506, 686